

Inhomogeneous Knight shifts induced by non-magnetic impurities in the Kagome antiferromagnet

Didier Poilblanc¹ and Arnaud Ralko²

¹ Laboratoire de Physique Théorique UMR5152, CNRS and Université de Toulouse, F-31062 France

² Institut Néel UPR2940, CNRS and Université de Grenoble, F-38000 France

(Dated: June 15, 2022)

The local perturbation induced by a non-magnetic impurity (described as a vacant site) in the quantum Heisenberg antiferromagnet on the kagome lattice is investigated using a generalized effective quantum dimer model approach. The modulations of the dimer density and of the local magnetization (induced by a finite magnetic field) are computed. The crystallization of two dimer bonds next to the vacancy is a robust feature which does not enable to discriminate between dimer liquid or valence bond crystal phases. In contrast, an analysis of the magnetization map further away from the impurity and a comparison of the resulting Nuclear Magnetic Resonance spectrum to the experimental one in Herbertsmithite clearly points towards a dimer liquid phase in this material.

Introduction – The spin-1/2 quantum Heisenberg antiferromagnet (QHAF) on the kagome lattice (see Fig. 1(a)) is believed to be the paradigm of frustrated quantum magnetism. It is also the best candidate to observe exotic (non-magnetically ordered) phases predicted by theorists. Among those, an algebraic spin liquid [1], a gapped dimer –or spin– liquid [2, 3] or a number of valence bond crystals (VBC) with 12-site [4], 18-site [5] and 36-site [5–7] unit cells or with columnar dimer order [8] have all been proposed as possible ground state (GS).

On the experimental side, Herbertsmithite [9] is an almost perfect realization of a kagome QHAF. In this material Copper atoms carrying spin-1/2 degrees of freedom are located on the sites of (very weakly coupled) kagome layers. In addition to the crystallographic structure, the closeness to an ideal system is supported by the remarkable *absence* of any magnetic ordering at the lowest attainable temperatures [10], as expected for a highly frustrated quantum magnet.

However, small deviations from a perfect kagome QHAF are known in this material. In addition to a small Dzyaloshinskii-Moriya (DM) anisotropy [11], Herbertsmithite contains a small amount of non-magnetic Zinc impurities substituting Copper atoms in the kagome planes. Nuclear Magnetic Resonance (NMR) offers a fantastic tool to probe impurities via the change induced by a nearby impurity on the local magnetic field at the nucleus whose resonance is being measured. The first estimations from NMR [12] of the Zinc concentration range from 6 to 10 %. It is not clear therefore, which experimental features in Herbertsmithite can really be attributed to intrinsic properties of the kagome QHAF and which of them are induced e.g. by Zinc substitution.

The goal of this work is to get deeper insights on the nature of the Herbertsmithite ground state (GS) from a quantitative analysis of the effects of spinless impurities. We start from a simple description of the material in terms of a SU(2)-symmetric kagome spin-1/2 QHAF, neglecting the small DM anisotropy. Within this description, recent calculations of NMR spectra [13] seem indeed to reflect some of the key experimental features [12]. On the other hand, the local susceptibilities (Knight shifts) obtained by high temperature series expansion [14] were claimed to agree with an algebraic (gapless) spin liquid phase. Here we provide an alternative

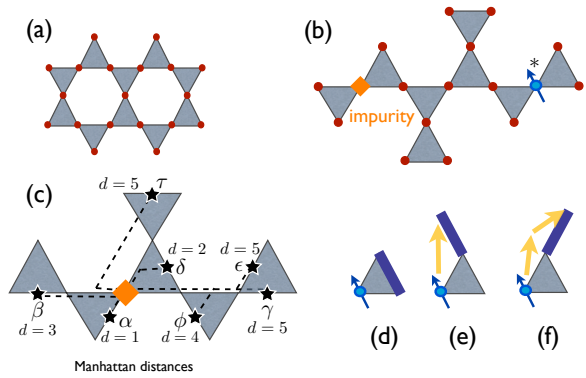


FIG. 1: (Color online). (a) Kagome lattice consisting of a hexagonal lattice of corner-sharing frustrated triangular units. The Heisenberg AFM interaction acts on all bonds of every triangle. (b) A non-magnetic impurity in the kagome lattice is described as a vacancy. Here we use $4\sqrt{3} \times 4\sqrt{3}$ ($N = 48$) and $5\sqrt{3} \times 5\sqrt{3}$ ($N = 75$) clusters containing a single impurity. (*) Only the $N = 48$ cluster contains a spinon. (c) The Manhattan distance d is obtained by counting the number of unit segments (oriented along the two crystallographic axis) on the path joining the impurity to a given bond center. Non-equivalent bonds are labelled by greek letters. (d) A spinon (carrying spin-1/2 shown by a blue arrow) on a triangle cannot hop on the sites of the same triangle. (e-f) A spinon can hop at further distances leading to a 120-degree (c) or 180-degree (back-flow) rotation (d) of the involved dimer.

analysis based on a generalized quantum dimer model (QDM) which give evidence that the experimental NMR data are consistent with a \mathbb{Z}_2 dimer liquid.

Theoretical description – Focussing on the diluted limit, it is legitimate to restrict to a single impurity [29]. The impurity is described as a vacant site as shown in Figs. 1(b,c). In other words, the bond exchange interaction $\mathbf{S}_i \cdot \mathbf{S}_j$ (in units of the exchange coupling J) acts on all bonds of the kagome lattice except on the four bonds connected to the impurity. Using Lanczos exact diagonalizations (LED) of small clusters of the kagome QHAF [15], it has been shown that a single impurity tends to ‘localize’ two singlet bonds next to it [16–18]. Although this local phenomenon is well captured even on very small clusters [13], LED of the QHAF do not al-

$$\begin{aligned}
\mathcal{H}_{\text{eff}} = & -J_6 \bigtriangleup \bigtriangleup - J_8 (\bigtriangleup \bigtriangleup + \bigtriangleup \bigtriangleup + \bigtriangleup \bigtriangleup) \\
& - J_{10} (\bigtriangleup \bigtriangleup + \bigtriangleup \bigtriangleup + \bigtriangleup \bigtriangleup) - J_{12} \bigtriangleup \bigtriangleup \\
& + V_6 \bigtriangleup \bigtriangleup + V_8 (\bigtriangleup \bigtriangleup + \bigtriangleup \bigtriangleup + \bigtriangleup \bigtriangleup) \\
& + V_{10} (\bigtriangleup \bigtriangleup + \bigtriangleup \bigtriangleup + \bigtriangleup \bigtriangleup) + V_{12} \bigtriangleup \bigtriangleup
\end{aligned}$$

FIG. 2: The effective QDM used here. A sum over all the hexagons of the lattice is implicit. Kinetic terms (J_α) promote cyclic permutations of the dimers around the loops and diagonal terms (V_α) count the numbers of “flippable” loops.

low to investigate reliably the perturbation of the media at larger distances from the impurity, which can be probed e.g. by NMR. Therefore, we shall use here an effective description based on the recently developed QDM allowing to handle larger clusters[19, 20]. Starting from a projection of the QHAF on the (non-orthogonal) NN singlet basis [21], one gets an effective QDM of the type shown in Fig. 2. Here we use the amplitudes obtained in Ref. [20], $V_6 = 1/5$, $V_8 = 2/63$, $V_{10} = 1/255$, $V_{12} = 0$, $J_6 = -4/5$, $J_8 = 16/63$, $J_{10} = -16/255$, $J_{12} = 0$ (in units of J) which defines our “Heisenberg” effective QDM H_{Heis} . An exactly solvable “Rokhsar-Kivelson” (RK) QDM H_{RK} defined by vanishing diagonal amplitudes $V_\alpha = 0$ and equal J_α kinetic amplitudes (set here to -1/4) has also been introduced [23]. Following Ref. 22, we shall consider a linear interpolation between the two Hamiltonians, $H_{\text{eff}}(\lambda) = \lambda H_{\text{Heis}} + (1 - \lambda) H_{\text{RK}}$.

Competing phases in the pure system – Prior to the study of the effect of an impurity, we provide first a brief summary of the results based on the QDM defined above (at zero magnetic field). Numerical results [22] show that a 36-site unit cell VBC is stabilized for $\lambda > \lambda_C \simeq 0.94$, in particular at the “Heisenberg” point $\lambda = 1$. A remarkable (topological) gapped \mathbb{Z}_2 dimer liquid which bears an exact analytical form at the RK point $\lambda = 0$ is stable for $\lambda < \lambda_C$. Besides, at exactly $\lambda = 1$, J_{12} vanishes so that the undetermined chiralities of the pinwheel (or star) resonances of the VBC pattern (see e.g. Ref. 22 for details) lead to an extra (Ising-like) macroscopic degeneracy. These findings at $\lambda = 1$ are in perfect agreement with recent series expansions on the QHAF [7]. However it should be stressed here that the derivation of the $\lambda = 1$ effective QDM is only semi-quantitative since it relies i) on the projection of the Heisenberg Hamiltonian onto the singlet subspace spanned by the NN VB and ii) it is subject to a (controlled) truncation of a series expansion. Besides, the real material might contain longer range exchange interactions. This suggests that a faithful description of the material in terms of a generalized QDM might not correspond exactly to the $\lambda = 1$ point. We therefore consider from now on λ as a “phenomenological” parameter and shall compare the experimental NMR data to theoretical results based on the extended Hamiltonian $H_{\text{eff}}(\lambda)$.

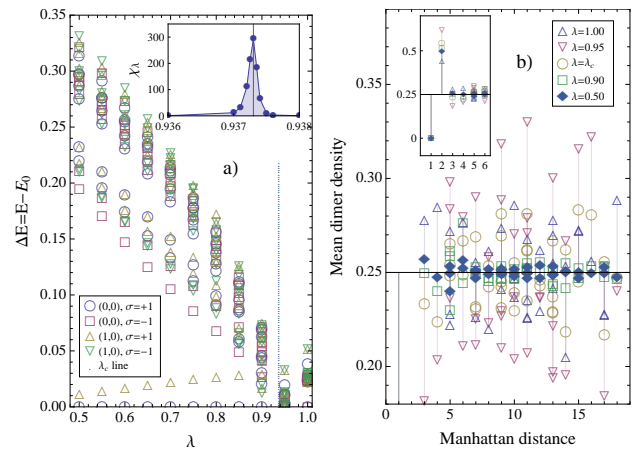


FIG. 3: (color online) (a) Spectrum versus λ of the effective QDM on a $N=75$ site periodic cluster containing a single impurity and with zero magnetization. The 8 lowest energy levels are shown in each of the 4 symmetry sectors. Inset: generalized susceptibility (see text) showing the location of the phase transition. For $\lambda < \lambda_C$, the large spectral gap above the quasi-degenerate topological GS correspond to the *single-vison* gap of the \mathbb{Z}_2 liquid. (b) Average dimer density versus Manhattan distance from the impurity on the same $N=75$ cluster. The short distance behavior is separated in the inset for clarity. The mean value corresponds to 1/4 dimer per bond.

Description of the single impurity results – We now consider inserting a single impurity. As stated above, we use the common modelisation of a spinless impurity (typically a Zinc atom substituted for copper) in terms of a vacant site as shown in Figs. 1(b,c). In the framework of the generalized QDM, the vacancy primarily suppresses the resonant and diagonal terms of Fig. 2 whose loop contains the vacancy site [30].

In the diluted impurity limit, one does not expect to fundamentally modify the *bulk* properties of the quantum magnet. To test this, we have considered a large $5\sqrt{3} \times 5\sqrt{3}$ periodic cluster of $N = 75$ sites with a single impurity (to comply with the hard-core dimer constraints such a cluster has to contain an odd number of sites) [24]. The full spectrum of this cluster is shown in Fig. 3(a) as a function of the parameter λ . Here we have distinguished between the four topological sectors (for such a torus topology) [31] and used the reflection symmetry w.r.t. one of the C_2 -axis passing through the impurity site ($\sigma = \pm 1$). A quantum phase transition [25] occurs as a function of λ for $\lambda = \lambda_C \simeq 0.9373$ as evidence from the sharp peak in the GS generalized susceptibility $\chi_\lambda = \partial^2 E_{\text{GS}} / \partial \lambda^2$ shown in the inset [26]. A topological \mathbb{Z}_2 liquid (with four-fold degeneracy on a torus) is stable for $\lambda < \lambda_C$. At $\lambda = \lambda_C$ the *single-vortex* (or “vison”) gap [32] corresponding to the first odd ($\sigma = -1$) energy excitation vanishes. For $\lambda > \lambda_C$ the system spontaneously breaks reflection symmetry (the GS is two-fold degenerate with $\sigma = \pm 1$ quantum numbers) as expected in the 36-sites VBC. These results and, in particular, the estimation of the critical value $\lambda_C \simeq 0.9373$ are fully consistent with the results obtained on a pure 108-sites clus-

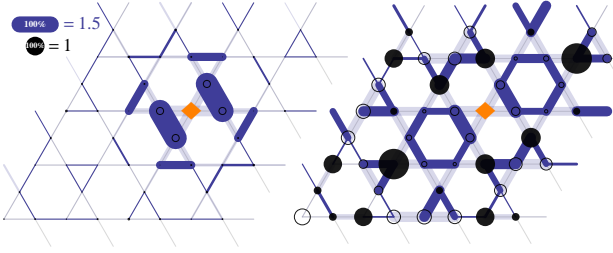


FIG. 4: (color online) Maps of the (relative) spatial fluctuations of the dimer density (segments) and site magnetization (circles) for $\lambda = 0.9$ (left) and $\lambda = 1$ (right) computed on a periodic $N = 48$ -site cluster with a single impurity and total magnetization $m/m_{\text{sat}} \sim 2\%$. Shown are the deviations from the average value normalized w.r.t. the average itself i.e. $(n_{ij} - n_{\text{ave}})/n_{\text{ave}}$ and $(m_i - m_{\text{ave}})/m_{\text{ave}}$, respectively. Light/dark (blue) segments and open/filled circles are used for negative/positive deviations from the average of the dimer density and the site magnetization, respectively.

ter [22].

It is interesting to examine the behavior of the dimer density as a function of the Manhattan distance (see Fig. 1(c)) from the impurity, as reported in Fig. 3(b) for different values of λ between 0.5 and 1. One striking feature is the large value of the dimer density on the two bonds facing the impurity (distance $d = 2$). This can be interpreted as a (singlet) *dimer crystallization* as found in prior studies of the Heisenberg quantum antiferromagnet [16–18]. Our study reveals that this phenomena is very robust and depends weakly on the supposed phase, liquid ($\lambda < \lambda_C$) or crystalline ($\lambda > \lambda_C$), of the model. Therefore this feature cannot be used practically as an experimental fingerprint. In contrast, when considering longer distances, strong differences in the bond modulation occur in the supposed liquid and VBC phases. For $\lambda < \lambda_C$, in the \mathbb{Z}_2 dimer liquid, the dimer density becomes very uniform beyond distance 1. When increasing λ the appearance of strong modulations is exactly correlated to the crossing of the critical value and the entering in the VBC phase. For $\lambda = 1$, the relative bond modulation amplitude is of order 20%.

Introducing a magnetic spinon – In an NMR setup a small magnetic field is applied to slightly polarize the system. The local site-dependent magnetization is then measured from the Knight shift. This setup can be realized theoretically by introducing an extra spin-1/2 (named “spinon” hereafter) as first proposed in Ref. 27. Physically, this spinon (polarized along the magnetic field) can be viewed as resulting from the breaking of a singlet bond by the introduction of the vacant site (impurity). The bond exchange interaction leads to the motion of the spinon. Here, we use the results for the spinon hoppings derived on the “Husimi cactus” i.e. neglecting the presence of closed loops in the lattice [28]. We believe this captures the main features resulting from the delocalization of the spinon. The spin hopping processes are shown in Fig. 1(d-f) and occur with an amplitude $-1/2$ (in units of J).

The maps of both the (bond) dimer density and the site mag-

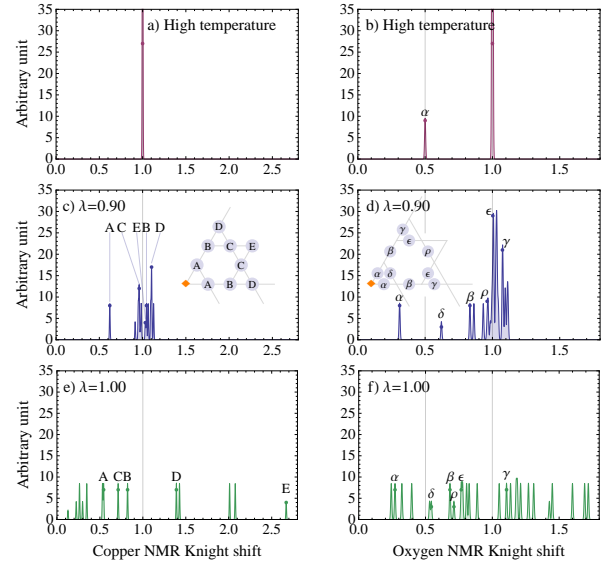


FIG. 5: (color online) Theoretical NMR spectra computed from the magnetization maps of Fig. 4. The Knight shift variables are normalized w.r.t. their high temperature values (fixing m/m_{sat}). Copper (a) and Oxygen (b) NMR spectra at high temperature. Zero-temperature Copper and Oxygen NMR spectra for $\lambda = 0.9$ (c,d) and $\lambda = 1$ (e,f). The impurity peaks are labelled according to the positions of the resonating nucleus shown in the insets (see also Fig. 1(c)).

netization computed on a $4\sqrt{3} \times 4\sqrt{3}$ (48-sites) cluster [24] are shown in Fig. 4 for $\lambda = 0.9 < \lambda_C$ and $\lambda = 1 > \lambda_C$. The dimer density map in this lightly polarized system is fully consistent with the previous zero field data of Fig. 3(b): the dimer liquid phase exhibits a very homogeneous dimer density apart from the two “crystallized” bonds next to the impurity while strong dimer patterns are clearly visible in the VBC phase. The local magnetization map is correlated with the dimer density map: for $\lambda = 0.9$ (liquid) the magnetization is slightly depressed on the four bonds NN to the impurity and very uniformly distributed beyond. For $\lambda = 1$ (VBC) a strong modulation in the local magnetization appears.

Comparison with experiments and conclusions – The different magnetization maps in the liquid and VBC phases are expected to lead to different characteristic NMR (theoretical) spectra which can be confronted to experiments in Herbertsmithite [12]. The theoretical Copper NMR spectra is defined by the histogram of the local site magnetizations. Since Oxygen is located between two coppers, the effective local magnetization is obtained by summing up the contributions from both sites (named here as *bond magnetization*). Both site and bond magnetization histograms have been computed for the same $\lambda = 0.9$ and $\lambda = 1$ values as used in Fig. 4, providing the theoretical Copper and Oxygen NMR spectra shown in Fig.5. For convenience, the Copper and Oxygen Knight shifts (x-axis) have been normalized w.r.t. their high temperature (bulk) values corresponding to a uniform spatial distribution of the magnetization. Note however that, even at $T \sim J$, the Oxygen nucleus located on the bonds connected to the impu-

ity site see only one Copper atom instead of two, yielding a small "satellite" peak in the spectrum of Fig. 5(b) at half the bulk Oxygen NMR shift. Decreasing temperature, this satellite peak remains well separated from the rest in the dimer liquid phase, while it merges with an increasingly broader spectrum in the VBC.

These results can be directly compared to the recently obtained ^{17}O NMR experimental results on the Kagome QHAF Herberthmithite which contains an intrinsic small Zinc substitution in the Copper Kagome planes [12]. Although the experimental NMR spectra are broaden by quadrupolar effects typical of powders, two separate structures can clearly be followed from high to low temperatures. The average shift of the "satellite" peak is roughly half of the main one. Hence, this peak has been interpreted as resulting from the resonance of the four Oxygen nucleus (labelled as " α " in Fig. 5) next to an impurity site. The experimental spectrum is therefore consistent with the theoretical Oxygen NMR spectrum [33] in the dimer liquid phase. In contrast, the strong dimer density modulation of the VBC phase ($\lambda = 1$) leads to a strong modulation of the local magnetization and a very broad NMR (Oxygen) NMR spectrum which can not be reconciled with the experimental one.

The fact that signatures of the expected VBC phase at $\lambda = 1$ are not seen in the Herberthmithite compound might have multiple origins, experimental and/or theoretical. Theoretically, the prediction of a VBC phase is based on an approximate (although controlled) framework and the location of the critical point λ_C , found to be very close to $\lambda = 1$, is only semi-quantitative. Besides, generalized QDM do not really provide a natural description for other candidates GS for the Kagome QHAF, as algebraic spin liquids. On the experimental side, a more realistic description of Herberthmithite may require to go beyond the simple NN QHAF. It is possible that longer range exchange interactions destabilize the VBC ground state in favor of the \mathbb{Z}_2 dimer liquid or some other candidate GS. It might also happen that the VBC phase is only stable at temperatures lower than those experimentally reached. Finally, we note that, experimentally, a large enough DM anisotropy [11] could fill the (spin) gap of the \mathbb{Z}_2 dimer liquid.

Acknowledgements – We thank G. Misguich and M. Mambrini for valuable discussions. We are deeply indebted to Fabrice Bert and Philippe Mendels for help in the understanding of their NMR data. D.P. acknowledges IDRIS (Orsay, France) for allocation of CPU time on the NEC supercomputer.

SU(N) VBC have been introduced by N. Read and S. Sachdev, Phys. Rev. B **42**, 4568 (1990).

- [6] P. Nikolic and T. Senthil, Phys. Rev. B **68**, 214415 (2003).
- [7] R.R.P. Singh and D.A. Huse, Phys. Rev. B **76**, 180407 (2007).
- [8] Ran Budnik and Assa Auerbach, Phys. Rev. Lett. **93**, 187205 (2004).
- [9] M. Shores, E. Nytka, B. Bartlett, and D. Nocera, J. Am. Chem. Soc. **127**, 13462 (2005).
- [10] P. Mendels et al., Phys. Rev. Lett. **98**, 077204 (2007).
- [11] A. Zorko et al., Phys. Rev. Lett. **101**, 026405 (2008).
- [12] A. Olariu et al., Phys. Rev. Lett. **100**, 087202 (2008).
- [13] Theoretical NMR spectra have been derived on a $N = 12$ sites cluster of the kagome QHAF with 2 impurities; See R. Chitra and M. J. Rozenberg, Phys. Rev. B **77**, 052407 (2008); M. J. Rozenberg and R. Chitra, Phys. Rev. B **78**, 132406 (2008).
- [14] K. Gregor and O. I. Motrunich, Phys. Rev. B **77**, 184423 (2008).
- [15] For recent numerical analysis of the pure kagome QHAF see G. Misguich and P. Sindzingre, J. Phys. Cond. Matt. **19**, 145202 (2007); P. Sindzingre and C. Lhuillier, Eur. Phys. Lett. **88**, 27009 (2009).
- [16] S. Dommange, M. Mambrini, B. Normand and F. Mila Phys. Rev. B **68**, 224416 (2003).
- [17] P. Sindzingre, C. Lhuillier, J.-B. Fouet, *Advances in Quantum Many-Body Theory*, vol. **5**, 90 (2002); *ibid, Int. J. of Modern Phys. B*, **17** (28), 5031 (2003).
- [18] Ioannis Rousouchatzakis et al., Phys. Rev. B **79**, 214415 (2009).
- [19] A. Ralko, M. Mambrini and D. Poilblanc, Phys. Rev. B **80**, 184427 (2009).
- [20] D. Schwandt, M. Mambrini and D. Poilblanc, Phys. Rev. B **81**, 214413 (2010); Note crucial differences with previous work, C. Zeng and V. Elser, Phys. Rev. B **51**, 8318 (1995).
- [21] The relevance of the NN VB basis is supported by LED of the (pure) QHAF revealing an exponential number (with N) of singlets below the spin gap. See M. Mambrini and F. Mila, Eur. Phys. J. B **17**, 651 (2000).
- [22] D. Poilblanc, M. Mambrini and D. Schwandt, Phys. Rev. B **81**, 180402 (2010).
- [23] G. Misguich, D. Serban, and V. Pasquier, Phys. Rev. Lett. **89**, 137202 (2002); see also D.S. Rohksar and S.A. Kivelson, Phys. Rev. Lett. **61**, 2376 (1988).
- [24] This cluster bears all discrete symmetries of the infinite kagome lattice. Although it does not accommodate the VBC 36-sites cell, it is believed to correctly capture the correct physics around the impurity.
- [25] This class of dimer liquid-VBC quantum phase transition can be described by a specific field theory. See C. Xu and S. Sachdev, Phys. Rev. B **79**, 064405 (2009).
- [26] S. Chen, L. Wang, Y. Hao and Y. Wang, Phys. Rev. A **77**, 032111 (2008).
- [27] A. Ralko, F. Becca and D. Poilblanc, Phys. Rev. Lett. **101**, 117204 (2008).
- [28] Z. Hao & O. Tchernyshyov, arXiv:1004:2293 (2010) and references therein.
- [29] In this limit, the magnetic response scales with the impurity concentration.
- [30] Other local resonances induced by the impurity itself exist but have negligible effects.
- [31] The (0,1), (1,0) and (1,1) sectors are degenerate. See Ref. 22 for details.
- [32] This contrasts with the case of the pure system where the spectral gap corresponds to a *double-vision* excitation. See Ref. 22.
- [33] We note that our analysis does not take the temperature dependence of the macroscopic susceptibility into account (we work at fixed global magnetization).

- [1] M. Hermele, Y. Ran, P.A. Lee and X.-G. Wen, Phys. Rev. B **77**, 224413 (2008).
- [2] P.W. Leung and Veit Elser, Phys. Rev. B **47**, 5459 (1993).
- [3] H. C. Jiang, Z. Y. Weng, and D. N. Sheng, Phys. Rev. Lett. **101**, 117203 (2009).
- [4] A. V. Syromyatnikov and S. V. Maleyev, Phys. Rev. B **66**, 132408 (2002).
- [5] J. B. Marston and C. Zeng, J. Appl. Phys. **69**, 5962 (1991);